Investigating cosmic stability through nonlinear perturbation and deceleration dynamics

Navya Jain, R.K. Mishra
Department of Mathematics, Sant Longowal Institute of Engineering and Technology, Longowal, 148106, Punjab, India
jainnavya008@gmail.com
ravkmishra@yahoo.co.in

(Submitted on 11.03.2026; Accepted on 15.06.2026)

Abstract. This paper investigates the stability of cosmological models within the framework of Brans–Dicke theory using a nonlinear perturbation approach. By employing a fractional quadratic deceleration parameter, we examine the dynamical evolution of perturbations and explore the interplay between stable and unstable modes in cosmological systems. To further support the theoretical analysis, the model is confronted with observational constraints through a statistical comparison with Hubble parameter data in order to obtain the best-fit values of the model parameters. Furthermore, the growth rate parameters are analyzed to characterize the behaviour of perturbations over cosmic time and to assess the long-term dynamical stability of the model. The results highlight the crucial role of nonlinear effects in determining cosmological stability and provide deeper insight into the mechanisms governing the stable and unstable evolutionary regimes of the universe.

Key words: BD theory, Deceleration parameter, Cosmic expansion, FLRW spacetime

1 Introduction

The investigation of cosmological models has been fundamental in gaining insight into the universe's large-scale structure and its evolution over time [Kirshner 2004]. These models attempt to describe the universe starting from its origin, through its present condition, and predict how it may evolve in the future. To do this, scientists use various theoretical approaches that provide new viewpoints to address key questions about the cosmos [Hayashi and Shirafuji 1979, Debono and Smoot 2016, Mishra and Jain 2024a, Jain et al. 2023]. Modified gravity theories are one such approach and have attracted interest due to their ability to explain phenomena that cannot be fully described by General Relativity (GR). These theories modify or extend GR to address its shortcomings and improve agreement with observations [Thirring 1961, Saez and Ballester 1986, Sotiriou and Faraoni 2010, Harko et al. 2011, Lazkoz et al. 2019, Mandal et al. 2020, Jain and Mishra 2025a, Sharma and Mishra 2026a].

A major reason for exploring theories beyond GR came from the discovery that the universe's expansion is accelerating. Observations such as Type Ia supernovae in the late 1990s [Perlmutter et al. 1999, Riess et al. 1998, Bennett et al. 2003], along with data from the cosmic microwave background (CMB) [Anderson et al. 2012, Hinshaw et al. 2013, Suzuki et al. 2012, Collaboration et al. 2014], support this accelerated expansion, which modified gravity models often explain more effectively.

One notable theory is the Brans–Dicke (BD) theory, developed by Carl Brans and Robert H. Dicke in 1961 [Brans and Dicke 1961]. This theory introduces a scalar field and allows the gravitational constant to vary, offering a more flexible description of gravity, especially in cosmology. In recent years, numerous cosmologists [Mishra and Sharma 2025, Mishra and Jain 2025b, Reddy and Vijaya 2015, Lu et al. 2019, Sharma and Mishra 2026b] have constructed cosmological models based on BD theory. Its adaptability makes it a valuable tool for studying the stability of cosmological solutions.

The stability of modified cosmological models is a key factor that must be examined carefully to verify their physical relevance. Perturbation theory has been very helpful in this context by analyzing how small disturbances change over time. Lifshitz [Lifshitz 1946] was among the pioneers who developed linear perturbation theory within GR, focusing on how small fluctuations behave in a uniform universe. This foundational work laid the basis for modern perturbation studies. Following this, other researchers [Springel et al. 2006] applied linear perturbation theory to explain the growth of cosmic structures. Bernardeau et al. [Bernardeau et al. 2002] extended these studies into the nonlinear domain to overcome the limits of the linear approach.

In our work, we study nonlinear perturbations by examining the growth rate parameter (GRP), which measures how perturbations grow or decay during both linear and nonlinear stability analyses. This method allows us to assess the long-term dynamical behaviour of cosmological models by applying small changes to the background solution and observing how the system responds to detect possible instabilities [Mishra and Jain 2024b]. This analysis also helps identify the ranges of parameters that yield stable models.

For this study, we use the Friedmann–Lemaître–Robertson–Walker (FLRW) metric, which assumes the universe is homogeneous and isotropic on large scales. It uses the scale factor $a(t)$ to represent cosmic expansion. The metric is written as:

$$ds^2 = c^2dt^2 - a^2(t)(dx^2 + dy^2 + dz^2)\,, \tag{1}$$

where t is cosmic time, and x, y, z are comoving coordinates. Time is measured in gigayears (Gyr). The Hubble parameter $H(t)$ and deceleration parameter (DP) $q(t)$ describe how the universe expands and are defined by:

$$H(t) = \frac{\dot{a}}{a}\,, \quad q(t) = -\frac{a\ddot{a}}{\dot{a}^2}\,.$$

We first derive the field equations for BD theory and find the background cosmological solution. Then, nonlinear perturbations are introduced, and the related continuity equation is derived to track their evolution. This approach helps us study the model's stability and understand its implications for cosmology.

In addition to determining the best-fit values of the model parameters, the proposed cosmological model is confronted with recent observational constraints. In particular, the model predictions are statistically tested against observational Hubble parameter $H(z)$ data to examine their consistency with cosmic expansion measurements. By reconstructing the Hubble function numerically and employing standard statistical techniques, the observational viability of the model parameters is assessed. This combined analytical and observational approach ensures that the proposed framework is not only dynamically stable but also compatible with current cosmological observations.

The paper is organized as follows: Section 2 presents the mathematical formulation of the cosmological model and solves the field equations. Section 3 describes the stability analysis using perturbation theory. Section 4 discusses the statistical validation with observational $H(z)$ dataset. Section 5 applies the findings to the model. Finally, Section 6 presents the conclusions and discussion. Our goal is to provide a better understanding of the universe's stability and the main factors that influence its evolution.

2 Mathematical Framework

In Einstein's General Theory of Relativity (GTR), both the gravitational constant G and the speed of light c are considered fixed constants. However, in 1961, Carl H. Brans and Robert H. Dicke introduced an extension of GTR that adds a scalar field—called the Brans-Dicke scalar field—alongside the metric tensor used in GR [Brans and Dicke 1961]. Unlike GR, where gravity's strength is constant, BD theory allows this strength to vary through the scalar field ϕ, which is connected to properties of spacetime. This idea is inspired by Mach's principle, which suggests that inertial effects arise from the influence of the entire mass in the universe. Therefore, particle masses are not absolute constants but depend on interactions with a universal field. Since gravitational acceleration, $\frac{Gm}{r^2}$, sets the scale for masses, the gravitational constant G should be related to the scalar field ϕ, which reflects the average mass density of the cosmos. This concept is encoded in the BD action by replacing G with ϕ^{-1}. Using natural units where $c = 1$, the BD Lagrangian density is expressed as:

$$\pounds = \frac{1}{16\pi} \int_\mu \left\{ \phi \left(R - \frac{w\phi_j \phi^j}{\phi^2} \right) \right\} \sqrt{-g}\, d^4x - \Lambda, \tag{2}$$

where, differing from the Einstein-Hilbert action, the factor multiplying R is $\frac{\phi}{16\pi}$ instead of $\frac{1}{16\pi G}$, consistent with $G \sim \phi^{-1}$. Here, $\phi_j = \frac{d\phi}{dx^j}$, R is the Ricci scalar, Λ the cosmological constant, w is the dimensionless Brans-Dicke coupling parameter controlling the interaction strength between gravity and the scalar field, and g is the determinant of the metric tensor g_{jk}. The terms involving ϕ describe its scalar character and coupling with matter.

Varying the action with respect to g_{jk} and ϕ, and setting $c = 1$, yields the following field equations:

$$R_{jk} - \frac{1}{2} R g_{jk} = -\frac{8\pi}{\phi} T_{jk} - \frac{w}{\phi^2} \left(\phi_{,j}\phi_{,k} - \frac{1}{2} g_{jk} \phi_{,l} \phi^{,l} \right) \tag{3}$$

$$-\frac{1}{\phi} \left(\phi_{;jk} - g_{jk} \right) - \Lambda g_{jk}, \tag{4}$$

where R_{jk} is the Ricci curvature tensor, T_{jk} the stress-energy tensor, and semicolons indicate covariant derivatives. The scalar field satisfies:

$$= \frac{8\pi}{3 + 2w} \left(T^j_j + A \right), \tag{5}$$

with $T^j_j \equiv T$ being the trace of T_{jk}, and $A = \frac{\Lambda\phi}{4\pi}$.

Using the FLRW metric and Einstein's stress-energy tensor, the dynamics of a homogeneous and isotropic universe can be modeled. The stress-energy tensor, representing matter and energy, is often treated as a perfect fluid:

$$T_{jk} = -pg_{jk} + (p+\rho)u_j u_k, \tag{6}$$

where ρ is energy density, p pressure, and u_j is the four-velocity vector satisfying $g_{jk}u^j u^k = 1$. In comoving coordinates, the fluid is at rest, so $u^j = (0,0,0,1)$. Scalar-tensor theories such as BD incorporate a scalar field ϕ alongside the metric tensor g_{jk}, governed by field equations that describe gravitational interactions. It is well-known that BD theory approaches GR in the limit $w \to \infty$ [Rama 1996, Rama and Ghosh 1996].

The Ricci tensor can be expressed in terms of the metric components as:

$$R_{jk} = \frac{\partial^2}{\partial x^j \partial x^k} \log\sqrt{-g} - \frac{\partial}{\partial x^l}\Gamma^l_{jk} + \Gamma^m_{jn}\Gamma^n_{mk} - \Gamma^l_{jk}\frac{\partial}{\partial x^l}\log\sqrt{-g}, \tag{7}$$

and the Ricci scalar is $R = g^{jk}R_{jk} = R^1_1 + R^2_2 + R^3_3 + R^4_4$. For the FLRW metric, $R = -6\left(\frac{\ddot{a}}{a} + \frac{\dot{a}^2}{a^2}\right)$. Substituting this into the BD field Eq. (3), and using the energy-momentum components $T^1_1 = T^2_2 = T^3_3 = -p, \quad T^4_4 = \rho$, we get the following equations for the flat FLRW universe:

$$\frac{2\ddot{a}}{a} + \frac{\dot{a}^2}{a^2} = \frac{-8\pi p}{\phi} - \frac{2\dot{\phi}\dot{a}}{a\phi} - \frac{w}{2}\frac{\dot{\phi}^2}{\phi^2} - \frac{\ddot{\phi}}{\phi} + \Lambda, \tag{8}$$

$$\frac{\dot{a}^2}{a^2} = \frac{8\pi\rho}{3\phi} - \frac{\dot{\phi}\dot{a}}{a\phi} + \frac{w\dot{\phi}^2}{6\phi^2} + \frac{\Lambda}{3}. \tag{9}$$

From the conservation of energy-momentum, $T^{jk}_{;k} = 0$, it follows that

$$\frac{d}{dt}(\rho a^3) + 3pa^2\dot{a} = 0. \tag{10}$$

The scalar field ϕ obeys the equation:

$$\frac{1}{a^3}\frac{d}{dt}\left(\dot{\phi}a^3\right) = \frac{8\pi}{2w+3}(\rho - 3p) - 3\Lambda. \tag{11}$$

3 Stability Analysis in the Brans-Dicke Cosmological Model

Stability analysis is an important tool to study how small disturbances change over time and space, helping to find out if a system remains steady, grows, or fades away. Its goal is to check whether the model keeps its form or if tiny changes can increase and cause major effects or instabilities. This type of analysis is especially relevant since the universe is constantly changing, and understanding stability under perturbations gives insight into both its early stages and long-term behaviour. Within BD theory, stability analysis is even more interesting because BD theory extends General Relativity by adding a scalar field ϕ that changes with time and location, along with the gravitational constant G, to reflect Mach's principle. The scalar field affects the structure of spacetime, leading to altered gravitational dynamics controlled by the BD parameter w, which measures how strongly the scalar field and gravity interact. While Nariai [Nariai 1969] provided an important first-order analysis, our study extends the framework by incorporating second-order perturbations, thereby offering a more comprehensive stability analysis within BD cosmology. This approach enables us to examine potential deviations from first-order predictions and test the robustness of the theory under higher-order perturbations. In this section, we use perturbation methods on the FLRW metric to examine the universe's stability, focusing on variations in density and pressure. The FLRW metric serves as a well-established framework describing the universe's large-scale structure, providing a basis to study departures from uniformity and isotropy. Using Eqs. (8)–(11), we obtain the continuity equation that includes terms for ρ, p, the Hubble parameter $\frac{\dot{a}}{a}$, the scalar field ϕ, and their higher-order derivatives as shown below

$$\left[8\pi(p+\rho)+(w+\frac{3}{2})\frac{\dot{\phi}^2}{\phi^2}\right]\frac{\dot{a}}{a}=-\frac{8\pi\dot{\rho}}{3}+\frac{4\pi\dot{\phi}}{3\phi}(\rho-3p)+\frac{\Lambda\dot{\phi}}{3}-\left(\frac{2w+3}{6}\right)\frac{\dot{\phi}\ddot{\phi}}{\phi} \tag{12}$$

Our continuity Eq. (12) involves ϕ, $\dot{\phi}$, and $\ddot{\phi}$, making it difficult to determine the evolution of ϕ independently without an additional condition. The scalar field evolution Eq. (5) includes contributions from the trace of the energy-momentum tensor and the cosmological constant, and is therefore highly coupled with the matter variables ρ, p, and the scalar field itself. Solving this equation analytically without an ansatz is, in general, non-trivial and leads to a complicated dynamical system. To make the system tractable and enable analytical exploration of cosmological behaviour, we adopt a power-law dependence of ϕ on the scale factor in the form $\phi \propto a^{\beta}$, motivated by earlier work [Johri and Desikan 1994]. This assumption connects the scalar field evolution to cosmic expansion in a physically reasonable way, considering that $\phi \sim G^{-1}$. It also acts as a closure condition to reduce the number of unknowns in the system. Therefore, following earlier works, we consider $\phi = \phi_0 a^{\beta}$, where β is a constant and ϕ_0 is the proportionality factor. This choice facilitates the analytical treatment of the model while preserving its physical relevance.

The continuity equation represents the conservation of energy in a universe that is expanding. It ensures that as the universe grows, the energy density and pressure change in a way that follows conservation rules. From Eqs. (12), we get the following expression:

$$\ddot{\rho}=\left(-Z\frac{\dot{a}}{a}+\beta-2A\right)\dot{\rho}-3\frac{\dot{a}}{a}Z\dot{p}+\frac{8\pi Z^2+32\pi ZA-8\pi Z\beta-16\pi\beta A+32\pi A^2}{\phi_0 a^\beta}\rho^2 + \frac{72\pi Z^2}{\phi_0 a^\beta}p^2+\left(2A\Lambda(Z-\beta+2A)-\frac{4A\Lambda}{6+6\beta-w\beta^2}\right)\rho + 6AZ\Lambda p+\frac{24\pi Z}{\phi_0 a^\beta}\left(2Z-\beta+4A\right)\rho p-\frac{A\Lambda^2}{2\pi}\phi_0 a^\beta\left(\frac{1}{6+6\beta-w\beta^2}-A\right), \tag{13}$$

where $Z=\frac{2+2\beta-\frac{w}{3}\beta^2}{2+\beta}$ and $A=\frac{2w\beta+3\beta^2+3\beta+6}{3(2+\beta)}$. We extend the perturbation study by including higher-order terms for energy density ($\delta\rho$) and pressure (δp). Unlike linear perturbation theory, which simplifies dynamics by linearizing around a background solution, the nonlinear framework incorporates complex interactions and higher-order couplings among perturbed variables. We apply the GRP analysis to examine the stability of the system under these nonlinear deviations. Our focus is on matter perturbations while assuming a fixed background metric, which facilitates the stability analysis. Since metric perturbations are not dynamically considered, gauge freedom has minimal effect on our results. Let X represent the set of cosmological variables, including energy density ρ and pressure p. These variables are perturbed as follows:

$$X(t)=X_0(t)+\delta X(t), \quad \text{where} \quad \delta X(t)=\sum_{n=1}^{\infty}\epsilon_n X^{(n)}(t)\,. \tag{14}$$

Here, $X_0(t)$ denotes the unperturbed background variables, ϵ_n are small expansion parameters, and $X^{(n)}(t)$ represent higher-order perturbation terms. The evolution equations for X in the cosmological model arise from Brans-Dicke theory as

$$\mathcal{F}(X,\delta X,\delta^2 X)=0\,, \tag{15}$$

where $\mathcal{F}$ includes nonlinear effects stemming from higher-order derivatives and couplings between ρ and p. By substituting the perturbation expansions into $\mathcal{F}$ and expanding up to second order, we get

$$\mathcal{F}_0(X_0)+\epsilon\mathcal{L}(\delta X)+\epsilon^2\mathcal{N}(\delta X,\delta X)=0\,, \tag{16}$$

with $\mathcal{L}$ as the linear operator and $\mathcal{N}$ capturing second-order nonlinear effects. To simplify, our analysis concentrates on the first two perturbation orders, crucial for evaluating the system's stability against disturbances. For the nonlinear perturbation, the perturbed variables are represented in a time-dependent form as $\delta X=\delta X_0 e^{\lambda t}$, where λ denotes the perturbation growth rate. Substituting these perturbed quantities back into the governing equations yields a system that can be expressed in matrix form as

$$\mathbf{M}.\delta=0\,,$$

where δ is a vector of perturbed quantities containing linear, quadratic, and higher-order terms, and $\mathbf{M}$ is the coefficient matrix. Using this, we obtain

$$\begin{bmatrix} m_{11} & 0 & 0 & 0 & 0 & 0 & 0 & 0 \\ 0 & m_{22} & 0 & 0 & 0 & 0 & 0 & 0 \\ 0 & 0 & m_{33} & 0 & 0 & 0 & 0 & 0 \\ 0 & 0 & 0 & m_{44} & 0 & 0 & 0 & 0 \\ 0 & 0 & 0 & 0 & m_{55} & 0 & 0 & 0 \\ 0 & 0 & 0 & 0 & 0 & m_{66} & 0 & 0 \\ 0 & 0 & 0 & 0 & 0 & 0 & m_{77} & 0 \\ 0 & 0 & 0 & 0 & 0 & 0 & 0 & m_{88} \end{bmatrix} \begin{bmatrix} (\delta\rho)^2 \\ (\delta p)^2 \\ \delta\rho \\ \delta p \\ (\delta\rho)^2\delta p \\ \delta\rho(\delta p)^2 \\ \delta\rho\delta p \\ (\delta\rho)^2(\delta p)^2 \end{bmatrix} = \begin{bmatrix} 0 \\ 0 \\ 0 \\ 0 \\ 0 \\ 0 \\ 0 \\ 0 \end{bmatrix} \tag{17}$$

where the diagonal elements are given as:

$$\begin{aligned} m_{11} &= 4\epsilon_1\lambda^2 + 2Z\epsilon_1\lambda\frac{\dot{a}}{a} - 2\beta\epsilon_1\lambda + 4A\epsilon_1\lambda - X_1\epsilon_1 - Y_1\epsilon_1 p_0\,, \\ m_{22} &= 6\frac{\dot{a}}{a}Z\epsilon_2\lambda - 6AZ\Lambda\epsilon_2 - Y_1\epsilon_2\rho_0\,, \\ m_{33} &= \lambda^2 + Z\lambda\frac{\dot{a}}{a} - \beta\lambda + 2A\lambda - X_1 - Y_1 p_0\,, \\ m_{44} &= 3\frac{\dot{a}}{a}\lambda Z - 6AZ\Lambda - Y_1\rho_0\,, \\ m_{55} &= -Y_1\epsilon_1\,, \quad m_{66} = -Y_1\epsilon_2\,, \quad m_{77} = -Y_1\,, \quad m_{88} = -Y_1\rho_0 p_0\,, \end{aligned}$$

where

$$\begin{aligned} X_1 &= 8\pi Z^2 + 32\pi ZA - 8\pi Z\beta - 16\pi\beta A + 32\pi A^2\,, \\ Y_1 &= \frac{24\pi Z}{\phi_0 a^\beta}(2Z - \beta + 4A)\,. \end{aligned}$$

Each m_{ii} contains the parameter λ, which governs the time evolution of perturbations. In order to determine the allowed values of λ, we consider the homogeneous system arising from the perturbation equations. The GRPs are obtained by requiring non-trivial solutions, which is achieved by imposing the condition $\det(\mathbf{M}) = 0$. In the present analysis, the perturbation matrix is assumed to be diagonal-dominant under a quasi-linear approximation, implying that higher-order cross-coupling terms between different perturbation modes are neglected compared with the dominant self-interaction contributions. This approximation preserves the essential nonlinear behaviour of the perturbation dynamics while keeping the resulting system analytically tractable. Consequently, the determinant condition leads to simplified characteristic relations for the individual perturbation modes. The stability of the system is determined by the sign of the real parts of the GRPs; in particular, perturbations remain bounded when the condition $\mathrm{Re}(\lambda_i) < 0$ is satisfied for all modes. Within the present framework, the determinant condition reduces to a consistency relation $Y_1 = 0$, which identifies special stability-compatible parameter configurations of the model. This yields the following expressions for the GRPs:

$$\lambda_1^{\pm} = -\frac{Z}{4}\frac{\dot{a}}{a} + \frac{1}{4} + \frac{3}{4}\sqrt{1+\frac{2w}{3}} - \frac{A\epsilon_2}{2\epsilon_1} \pm \frac{1}{4\epsilon_1}$$
$$\sqrt{Z^2\epsilon_1^2\left(\frac{\dot{a}}{a}\right)^2 + 2Z\epsilon_1(2A\epsilon_2 - \epsilon_1\beta)\frac{\dot{a}}{a} + \epsilon_1^2(\beta^2+4X_1) + 4A^2\epsilon_2^2 - 4A\beta\epsilon_1\epsilon_2}\,, \quad (18)$$

$$\lambda_2^{\pm} \quad = \quad -\frac{Z}{2}\frac{\dot{a}}{a} \; + \; \frac{\beta}{2} \; - \; A \; \pm \; \frac{1}{2}\sqrt{Z^2\left(\frac{\dot{a}}{a}\right)^2 + 2Z\left(2A-\beta\right)\frac{\dot{a}}{a} + 4(A^2 - A\beta + X_1)}\,, \quad (19)$$

$$\lambda_3 = \frac{A\Lambda}{6\frac{\dot{a}}{a}}\,. \quad (20)$$

Here $\lambda_1^{\pm}, \lambda_2^{\pm}$, and λ_3 represent the GRPs associated with the perturbation matrix $\mathbf{M}$. The condition $Y_1 = 0$ further constrains the model parameters and yields two admissible solutions for β:

$$\beta = 3 \pm 3\sqrt{1+\frac{2w}{3}}\,, \quad (21)$$

and

$$\beta = \frac{-4w-9}{9-2w} \pm \frac{1}{9-2w}\sqrt{(4w+9)^2 - (9-2w)36}\,. \quad (22)$$

These constraints on β arise from the underlying BD scalar–tensor coupling structure embedded in the perturbation matrix, and therefore they encode the dynamical consistency of the scalar field sector with the background cosmological evolution. Hence, the allowed ranges of β directly reflect the stability requirements of the BD framework under nonlinear perturbations. These values of β are subsequently used in the stability analysis of the cosmological model.

4 DP and Statistical Validation with Observational $H(z)$ Data

Studying the signs and sizes of the GRPs helps us understand the stability of the cosmological model. This method allows us to classify whether the universe is stable or unstable under small disturbances and also gives a sense of how quickly stability or instability develops. A positive λ means at least one perturbation grows exponentially, showing instability, while $\lambda = 0$ indicates a borderline stable state with perturbations staying constant or changing slowly. If λ is negative, perturbations die out over time, indicating stability for the corresponding perturbation mode. In this section, we apply the GRP-based stability analysis to the models we propose.

The DP is an important quantity for understanding how the universe expands. It shows whether the expansion is slowing down ($q > 0$) or speeding up ($q < 0$). Observations from Type Ia supernovae support the idea of a transition in cosmic expansion [Riess et al. 1998, Bennett et al. 2003, Anderson et al. 2012]. Various parametrizations of the DP have been proposed in the literature. For example, Berman [Berman and Mello 1988] studied constant DP models, Akarsu and Dereli [Akarsu and Dereli 2012] introduced a linear varying DP, and Mishra et al. [Jain and Mishra 2025b, Jain and Mishra 2025c, Sharma and Mishra 2026c] examined a bilinear DP to better describe cosmic evolution.

Our continuity equation depends on the scale factor $a(t)$ and its derivatives, which are key to understanding how cosmic parameters change. To solve the system exactly, we need a specific form for $a(t)$. Without this, the system cannot be fully solved, making it hard to get useful physical results. Specifying a suitable form of the DP $q(t)$ enables the determination of the scale factor $a(t)$. Since q measures how the universe's expansion changes over time, adopting an appropriate form of $q(t)$ lets us derive $a(t)$ in a consistent way. Based on the known behaviour of q changing sign and supported by earlier studies, we use a fractional quadratic form:

$$q(t) = -\frac{a\ddot{a}}{\dot{a}^2} = \frac{\alpha(1-t^2)}{1+t^2}\,, \tag{23}$$

where α is an arbitrary constant chosen to reflect the dynamical evolution of the universe. From Eq. (23), the Hubble parameter is obtained as

$$H(t) = \frac{\dot{a}}{a} = \frac{1}{(1+\alpha)t + 2\alpha\tan^{-1} t}\,. \tag{24}$$

To reconstruct the scale factor $a(t)$, we note that the expression for $H(t)$ involves non-trivial functional forms containing inverse trigonometric terms, which do not admit a simple exact closed-form integration. To obtain an analytically tractable expression, we employ a series expansion approach. Specifically, $H(t)$ is expanded about $t=0$, and the resulting series is integrated term by term. The exponential form of the integrated series is then reconstructed and subsequently expanded, retaining terms up to a finite order (up to $\mathcal{O}(t^6)$). Therefore, the resulting expression for $a(t)$ represents an approximate analytical solution derived from a truncated series expansion.

$$a(t) = (t-\alpha t)^{\frac{1}{1-\alpha}} e^{\frac{-\alpha t^2\left(1890(-1+\alpha)^2+63(-1+\alpha)(9+\alpha)t^2+2(135-18\alpha+23\alpha^2)t^4\right)}{5670(-1+\alpha)^4}}\,. \tag{25}$$

To assess the physical viability and observational relevance of our proposed cosmological model with a time-dependent DP, and to determine the best-fitted values of the unknown parameter, mainly α, we perform a comprehensive statistical analysis using the latest observational Hubble parameter dataset $H(z)$ compiled by Moresco et al. [Moresco et al. 2022]. The combined approach allows us to bridge the gap between theoretical predictions and observational data. Several recent studies have employed Hubble datasets to constrain alternative cosmological models, especially those aiming to explain late-time cosmic acceleration without invoking a strictly constant cosmological constant [Jain and Mishra 2026a, Galbany et al. 2023, Dhawan et al. 2018, Jain and Mishra 2026b, Huang et al. 2020, Sharma and Mishra 2026d]. For the observational analysis, it is often convenient to reformulate cosmological quantities in terms of the redshift z, which directly encodes the expansion history of the Universe and is related to the cosmic scale factor through the relation

$$1+z = \frac{a_0}{a(t)}\,, \tag{26}$$

where a_0 denotes the present value of the scale factor. Since the scale factor obtained in Eq. (25) is expressed explicitly as a function of cosmic time t, an analytical inversion to obtain $t(z)$ is not straightforward. Therefore, the cosmological field equations were reformulated in terms of the coupled differential equations

$$\frac{dH}{dz} = \frac{(1+q)}{1+z}H\,, \qquad \frac{dt}{dz} = -\frac{1}{(1+z)H}\,, \tag{27}$$

where the DP $q(t)$ is substituted from the chosen parametrization. These equations were numerically solved using the MATLAB `ODE45` solver to reconstruct the theoretical Hubble parameter corresponding to each observational redshift point. The theoretical Hubble parameter employed in the statistical analysis is defined as

$$H_{\text{th}}(z) \equiv H(z;\alpha, H_0)\,, \tag{28}$$

where $H_{\text{th}}(z_i;\alpha, H_0)$ represents the theoretical Hubble parameter obtained after numerically solving the coupled differential equations for the adopted form of the DP. Since the parametrization of $q(t)$ depends explicitly on the parameter α, the observational fitting constrains only the parameters α and the present Hubble constant H_0. The parameters w and β do not explicitly appear in the reconstructed Hubble function. Consequently, they were not included as free parameters in the observational fitting procedure. The BD parameter w was explored independently in the range $0 \leq w \leq 5$ during the subsequent stability analysis, while the corresponding values of β were determined from the stability condition $Y_1 = 0$, yielding the admissible solutions given in Eqs. (21) and (22). To determine the best-fit values of the model parameters, the standard chi-square minimization technique was employed:

$$\chi^2 = \sum_i \frac{\left[H_{\text{obs}}(z_i) - H_{\text{th}}(z_i;\alpha, H_0)\right]^2}{\sigma_i^2}\,, \tag{29}$$

where $H_{\text{obs}}(z_i)$ and σ_i denote the observed Hubble parameter values and their corresponding uncertainties, respectively. The minimization procedure was carried out using the Sequential Quadratic Programming (SQP) algorithm through the MATLAB `fmincon` routine. The resulting best-fit values were obtained as

$$\alpha = 0.09\,, \qquad H_0 = 63.608\ \text{km}\,\text{s}^{-1}\text{Mpc}^{-1}\,, \tag{30}$$

with a minimum chi-square value $\chi^2 = 18.074$. Since the total number of observational data points is $N = 32$ and the number of fitted parameters is $K = 2$, the number of degrees of freedom becomes $\text{dof} = N - K = 30$. Consequently, the reduced chi-square parameter is obtained as $\chi^2_\nu = \frac{\chi^2}{\text{dof}} = 0.602$. The reduced chi-square value smaller than unity may indicate that the observational uncertainties are slightly overestimated or that the model provides a statistically good fit to the available data. To further evaluate the statistical performance of the model, the Akaike Information Criterion (AIC) and Bayesian Information Criterion (BIC) were also calculated. These criteria are commonly used in cosmology to compare the goodness of fit while penalizing unnecessary model complexity. They are defined as

$$\text{AIC} = \chi^2 + 2K\,, \tag{31}$$

and

$$\mathrm{BIC} = \chi^2 + K \ln N\,, \tag{32}$$

where K denotes the number of free model parameters and N represents the total number of observational data points. For the present model, the obtained values are

$$\mathrm{AIC} = 22.074\,, \qquad \mathrm{BIC} = 25.006\,. \tag{33}$$

For comparison, the standard flat ΛCDM cosmological model was also constrained using the same observational $H(z)$ dataset by simultaneously fitting the parameters H_0 and Ω_m. The corresponding Hubble parameter for the ΛCDM model is given by

$$H(z) = H_0\sqrt{\Omega_m(1+z)^3 + (1-\Omega_m)}\,. \tag{34}$$

The statistical results obtained for both models are summarized in Table 1. To quantify the statistical difference between the two cosmological models, the

Table 1: Statistical comparison of the present model with the standard ΛCDM cosmology using observational $H(z)$ data.

Parameter	Present Model	ΛCDM
H_0 ($\mathrm{km\,s^{-1}Mpc^{-1}}$)	63.608	68.160
α	0.09	–
Ω_m	–	0.3189
χ^2	18.074	14.554
χ^2_ν	0.602	0.485
AIC	22.074	20.554
BIC	25.006	23.486

relative information criteria were evaluated as

$$\Delta\mathrm{AIC} = \mathrm{AIC} - \mathrm{AIC}_{\Lambda\mathrm{CDM}} = 1.520\,, \tag{35}$$

and

$$\Delta\mathrm{BIC} = \mathrm{BIC} - \mathrm{BIC}_{\Lambda\mathrm{CDM}} = 1.520\,. \tag{36}$$

Since both ΔAIC and ΔBIC are smaller than 2, the present cosmological model exhibits statistical support comparable to the standard ΛCDM cosmology. Therefore, the proposed model remains observationally viable and statistically competitive when constrained with the observational $H(z)$ dataset.

A Metropolis–Hastings Markov Chain Monte Carlo (MCMC) analysis was further performed using the same observational $H(z)$ dataset in order to estimate the posterior distributions and confidence intervals of the free model parameters. Flat priors were imposed on the parameters within the ranges $-5 \le \alpha \le 5$, $40 \le H_0 \le 100$ $\mathrm{km\,s^{-1}Mpc^{-1}}$. Since the adopted parametrization of the DP depends explicitly only on α, the observational $H(z)$ fitting constrains only the parameters α and H_0. The remaining model parameters, namely β and w, do not explicitly appear in the reconstructed Hubble function $H(z)$ and were not included among the MCMC fitting parameters. The posterior constraints obtained from the MCMC analysis are

$$\alpha = -0.0202 \pm 0.1356\,, \qquad H_0 = 62.083 \pm 2.881\ \mathrm{km\,s^{-1}Mpc^{-1}}\,. \tag{37}$$

The marginally negative central value of α obtained from the MCMC analysis does not indicate any inconsistency, since the corresponding confidence interval also includes positive values of α. This suggests that the observational $H(z)$ dataset permits a narrow range of both small positive and negative values around $\alpha \approx 0$, while still remaining statistically consistent with the accelerated expansion behaviour predicted by the model. Fig. 1 presents a graphical

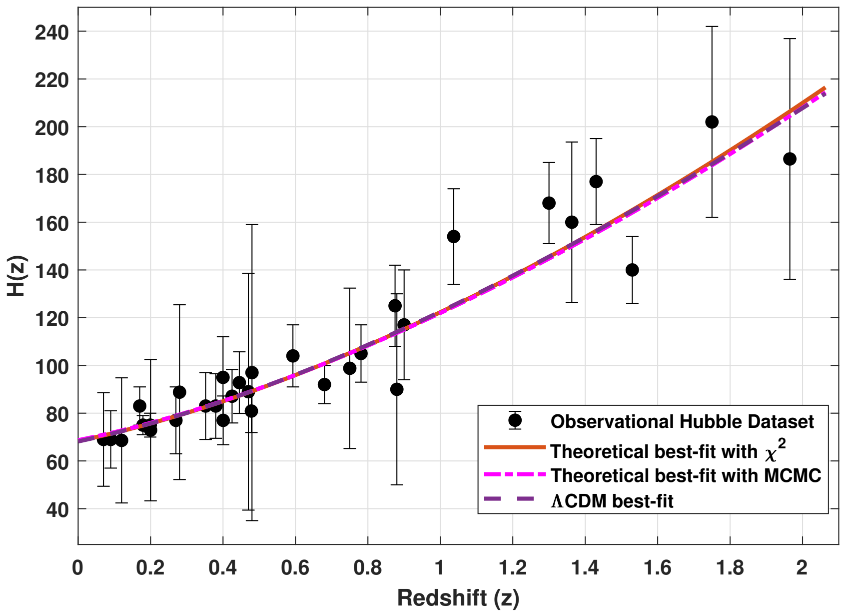

Fig. 1: Graphical representation of the Hubble observations, including error bars, alongside the optimal fit derived through χ^2 and MCMC statistical techniques for the theoretical model, and the predictions from the ΛCDM framework.

comparison between the observed Hubble parameter data and the theoretical predictions of the proposed model, constrained using both the χ^2 minimization and MCMC statistical techniques, along with the standard ΛCDM scenario. A close agreement between the observational measurements and the theoretical predictions is evident. Moreover, the figure demonstrates that the proposed framework maintains good accuracy over the entire redshift range, highlighting

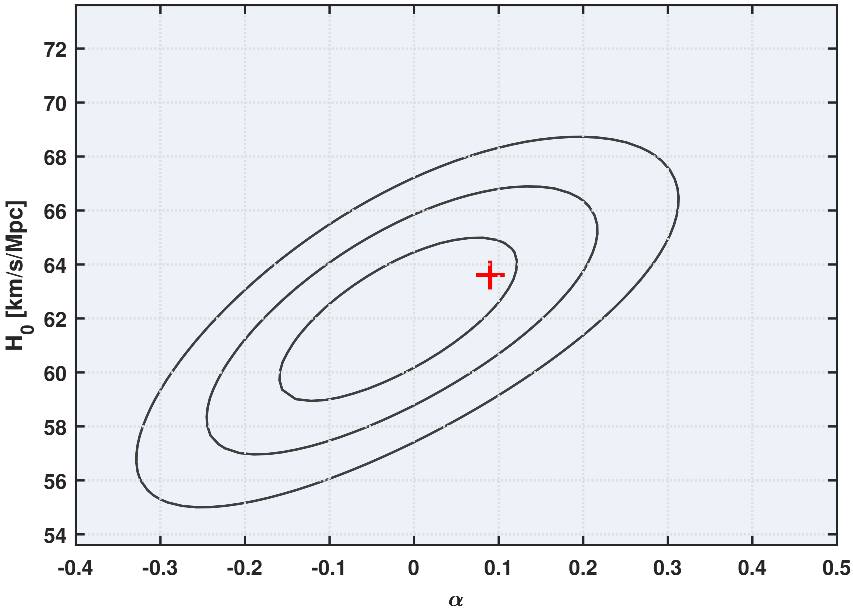

Fig. 2: Joint confidence contours in the (α, H_0) parameter space obtained from the observational $H(z)$ dataset using the χ^2 statistical analysis. The shaded regions represent the 1σ, 2σ, and 3σ confidence levels, while the red cross denotes the best-fit values of the model parameters.

its robustness and predictive consistency. Fig. 2 illustrates the joint confidence contours in the (α, H_0) parameter plane obtained from the observational $H(z)$ data. The shaded regions correspond to the 1σ, 2σ, and 3σ confidence intervals, whereas the red cross indicates the best-fit point. It is evident that the best-fit parameters lie well within the statistically allowed regions, demonstrating the consistency and observational viability of the proposed cosmological model with the current $H(z)$ measurements. For the subsequent analysis, we adopt the best-fit value $\alpha = 0.09$. This allows us to proceed with a consistent parameter choice for analyzing the expansion dynamics within our cosmological framework. The use of these values therefore ensures consistency between the model formulation and its observational reconstruction, without loss of generality.

5 GRP-Based Stability Analysis

In this Section, we analyze the dynamical behaviour of the cosmological model for different values of the parameter α. Fig. 3 illustrates the evolution of the DP and the Hubble parameter with cosmic time t for $\alpha = 0.09, 0.5$, and 1. As cosmic time evolves, the DP undergoes a transition from positive to negative values, indicating a transition from a decelerating to an accelerating phase of the universe. Meanwhile, the Hubble parameter approaches a small positive value at late times, consistent with an expanding universe. Next, to analyze

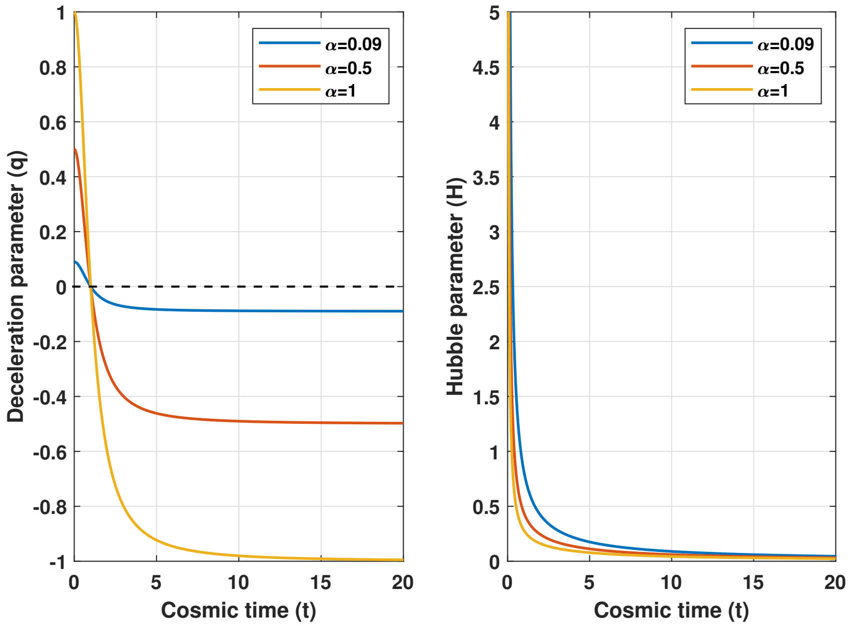

Fig. 3: Evolution of the DP and Hubble parameter with cosmic time t.

the stability of the cosmological model, different values of the parameter β are considered in the following subsections. Although Fig. 3 illustrates the qualitative behaviour of the cosmological dynamics for different values of α, the subsequent GRP-based stability analysis is performed using the observationally constrained best-fit value $\alpha = 0.09$ obtained from the statistical analysis of the $H(z)$ dataset.

Case 1: For $\boldsymbol{\beta = 3 + 3\sqrt{1 + \frac{2w}{3}}}$

Using $\beta = 3 + 3\sqrt{1 + \frac{2w}{3}}$ and substituting the values of a and $\frac{\dot{a}}{a}$ into the Eqs. (18)-(20), and solving for the $\lambda_1^{\pm}, \lambda_2^{\pm}$, and λ_3, we obtain the following expressions

$$\lambda_1^{\pm} = \frac{1}{4}\left(1 + \sqrt{9+6w} - \frac{Z}{t+\alpha t - 2\alpha tan^{-1}t} - \frac{2A\epsilon_2}{\epsilon_1}\right) \pm \frac{1}{4}\sqrt{\begin{aligned}&6\left(w+3+\sqrt{9+6w}+\tfrac{2}{3}X_1\right) + \tfrac{Z^2}{(t+\alpha t-2\alpha\tan^{-1}t)^2} \\ &-12A\left(1+\sqrt{1+\tfrac{2w}{3}}\right)\tfrac{\epsilon_2}{\epsilon_1} + 4A^2\tfrac{\epsilon_2^2}{\epsilon_1^2} - T^{'}\end{aligned}} \tag{38}$$

$$\lambda_2^{\pm} = \frac{1}{2}\left(3 - 2A + \sqrt{9+6w} - \frac{Z}{t+\alpha t - 2\alpha tan^{-1}t}\right) \pm \frac{1}{2}\sqrt{\begin{aligned}&\frac{Z^2}{(t+\alpha t - 2\alpha tan^{-1}t)^2} - \frac{2(3-2A+\sqrt{9+6w})Z}{t+\alpha t - 2\alpha tan^{-1}t} \\ &+4(A(-3+A-\sqrt{9+6w})+X_1)\end{aligned}} \tag{39}$$

$$\lambda_3 = \frac{A((1+\alpha)t + 2\alpha tan^{-1}t)\Lambda}{6}, \tag{40}$$

where $T^{'} = \frac{2Z\left(\epsilon_1(3+\sqrt{9+6w})-2A\epsilon_2\right)}{(t+\alpha t-2\alpha tan^{-1}t)\epsilon_1}$. Since ρ_0 and p_0 represent the equilibrium

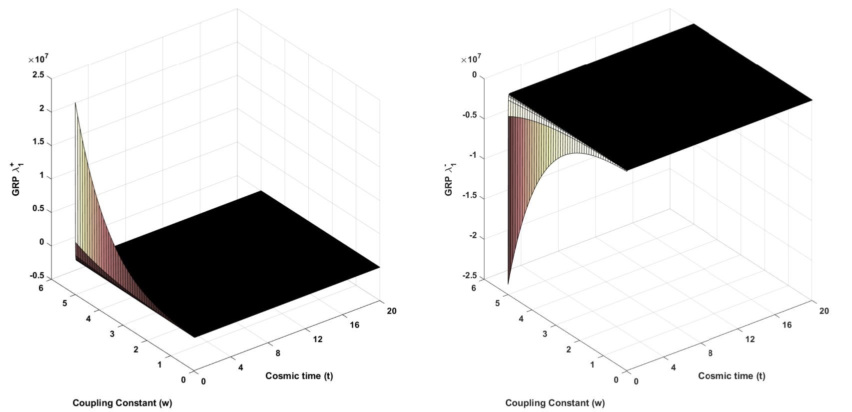

Fig. 4: λ_1^+ & λ_1^-'s visualization w.r.t cosmic time (t) and coupling constant w.

values, we set $p_0 = -\rho_0$ to model a universe dominated by the cosmological constant. Figs. 4, 5, and 6 illustrate the evolution of all five GRPs over cosmic time. At first, λ_1^+ and λ_2^+ are positive, indicating a brief unstable phase where perturbations grow quickly and push the system away from equilibrium. As time goes on, these positive growth rates, along with the initially negative ones, become negative. This transition indicates that the perturbations gradually decay with cosmic evolution, driving the system toward stability. The persistence of negative GRPs at late times ensures the exponential suppression of perturbations, gradually returning the system to equilibrium. This

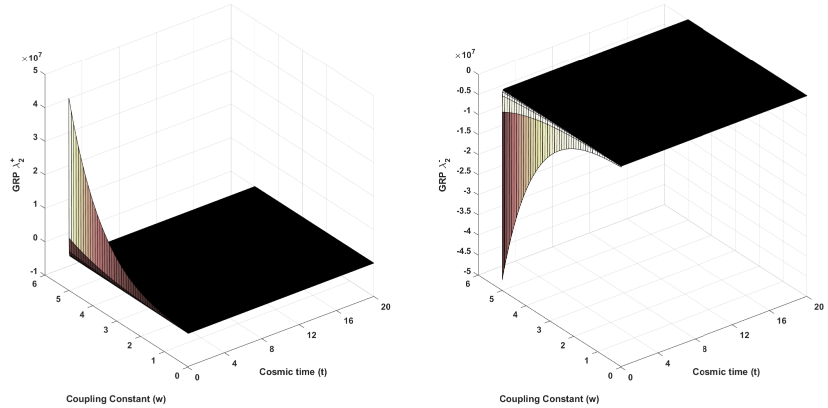

Fig. 5: λ_2^+ & λ_2^-'s visualization w.r.t cosmic time (t) and coupling constant w.

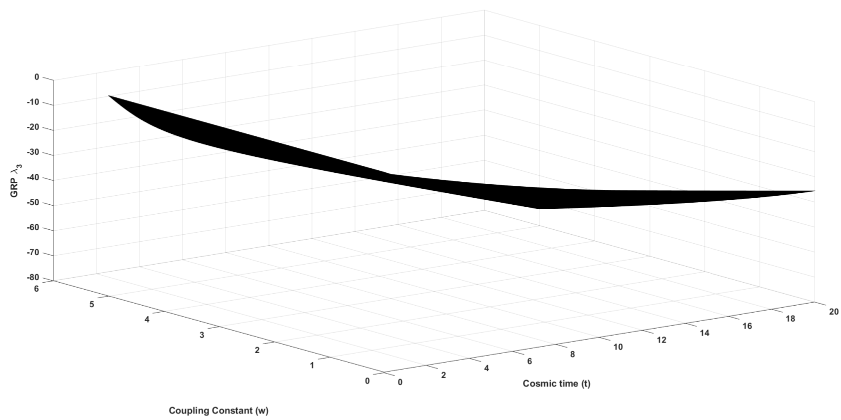

Fig. 6: λ_3's visualization w.r.t cosmic time (t) and coupling constant w.

pattern demonstrates the system's stability and its ability to recover from disturbances. In the long run, the negative growth rates dominate, confirming that the cosmological model remains stable and tends to settle back to a balanced state despite initial disruptions.

Case 2: For $\boldsymbol{\beta = 3 - 3\sqrt{1 + \frac{2w}{3}}}$

Using $\beta = 3 - 3\sqrt{1 + \frac{2w}{3}}$ and substituting the values of a and $\frac{\dot{a}}{a}$ into the Eqs. (18)-(20), and solving for the GRPs $\lambda_1^{\pm}, \lambda_2^{\pm}$, and λ_3, we obtain the following expressions

$$\lambda_1^{\pm} = \frac{1}{4}\left(1+\sqrt{9+6w} - \frac{Z}{t+\alpha t - 2\alpha\tan^{-1}t} - \frac{2A\epsilon_2}{\epsilon_1}\right)$$
$$\pm\frac{1}{4\epsilon_1}\sqrt{\begin{array}{r}6\epsilon_1^2\left(w+3-\sqrt{9+6w}+\frac{2}{3}X_1\right)+\frac{\epsilon_1^2 Z^2}{(t+\alpha t-2\alpha tan^{-1}t)^2}\\ -12A\epsilon_1(1-\sqrt{1+\frac{2w}{3}})\epsilon_2+4A^2\epsilon_2^2+T\end{array}} \quad (41)$$

$$\lambda_2^{\pm} = \frac{1}{2}\left(3-2A-\sqrt{9+6w} - \frac{Z}{t+\alpha t - 2\alpha tan^{-1}t}\right)$$
$$\pm\frac{1}{2}\sqrt{\begin{array}{r}\frac{Z^2}{(t+\alpha t-2\alpha tan^{-1}t)^2}+\frac{2(-3+2A+\sqrt{9+6w})Z}{t+\alpha t-2\alpha tan^{-1}t}\\ +4(A(-3+A+\sqrt{9+6w})+X_1)\end{array}} \quad (42)$$

$$\lambda_3 = \frac{A((1+\alpha)t+2\alpha tan^{-1}t)\Lambda}{6} \quad (43)$$

where, $T = \frac{2\epsilon_1 Z\left(\epsilon_1(-3+\sqrt{9+6w})+2A\epsilon_2\right)}{t+\alpha t-2\alpha tan^{-1}t}$.

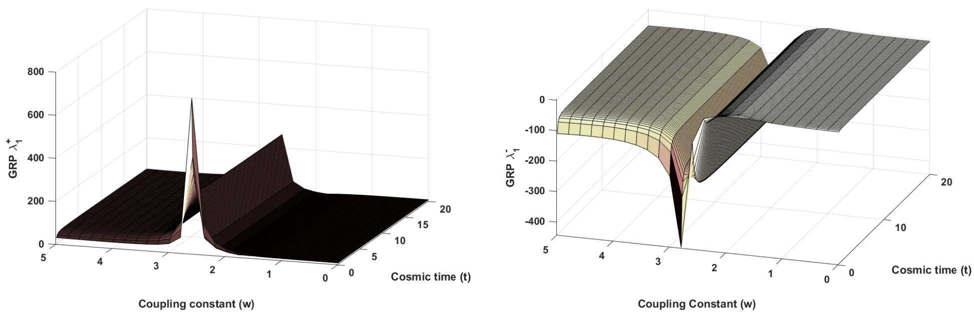

Fig. 7: λ_1^+ and λ_1^- visualizations with respect to cosmic time (t) and coupling constant w.

In Case-2, with $\beta = 3-3\sqrt{1+\frac{2w}{3}}$, for cosmic time $0 \le t \le 20$ and coupling constant $0 \le w \le 5$, Figs. 7, 8, and 9 illustrate the behaviour of the GRPs. From the graphical analysis, the parameters λ_1^+ and λ_2^+ remain positive throughout the considered cosmic evolution, indicating the presence of continuously growing perturbation modes. On the other hand, λ_1^- and λ_2^- remain negative, corresponding to decaying perturbations and hence stable perturbation modes.

The parameter λ_3 initially possesses positive values during the early cosmic phase, indicating transient instability, but gradually becomes negative at later times, suggesting that this perturbation mode eventually stabilizes as the universe evolves.

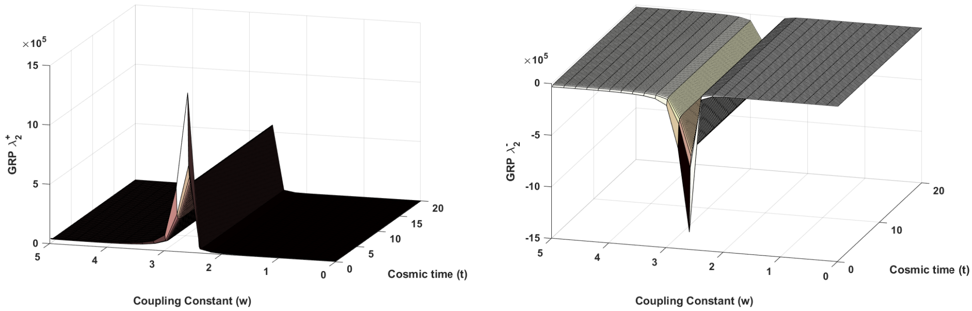

Fig. 8: λ_2^+ & λ_2^-'s visualization w.r.t cosmic time (t) and coupling constant w

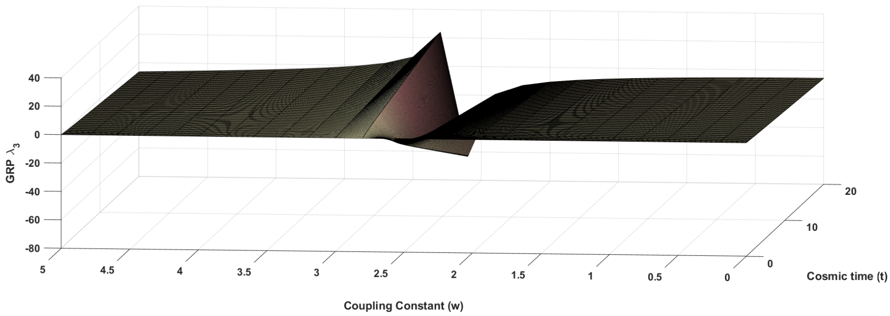

Fig. 9: λ_3's visualization w.r.t cosmic time (t) and coupling constant w

Although some perturbation modes exhibit stable behaviour, the persistence of positive GRPs, particularly λ_1^+ and λ_2^+, implies that the the complete cosmological system does not satisfy the stability criterion for all modes simultaneously. Therefore, Case-2 corresponds to an unstable cosmological configuration within the present perturbative framework.

Case 3: For $\boldsymbol{\beta = \frac{-4w-9}{9-2w} + \frac{1}{9-2w}\sqrt{(4w+9)^2-(9-2w)36}}$

Using $\beta = \frac{-4w-9}{9-2w} + \frac{1}{9-2w}\sqrt{(4w+9)^2-(9-2w)36}$ and substituting the values of a and $\frac{\dot{a}}{a}$ into the Eqs. (18)-(20), and solving for the $\lambda_1^{\pm}$, $\lambda_2^{\pm}$, and λ_3, we obtain the following expressions

$$\begin{aligned}\lambda_1^{\pm} = \frac{1}{4}\Bigg(1+\sqrt{9+6w} - \frac{Z}{t+\alpha t - 2\alpha tan^{-1}t} - \frac{2A\epsilon_2}{\epsilon_1}\Bigg) \\ \pm \frac{1}{4\epsilon_1}\sqrt{\begin{aligned}\epsilon_1^2\Bigg(\frac{(-9-4w+\sqrt{-243+144w+16w^2})^2}{(9-2w)^2}+4X_1\Bigg) \\ +\frac{\epsilon_1^2 Z^2}{(t+\alpha t-2\alpha tan^{-1}t)^2} + \frac{4\epsilon_1 A(T_1)\epsilon_2}{-9+2w} + T_2\end{aligned}}\end{aligned} \tag{44}$$

$$\lambda_2^{\pm} = \frac{1}{2}\Big(- 2A + \frac{9+4w}{-9+2w} + \frac{\sqrt{-243+144w+16w^2}}{9-2w} - \frac{Z}{t+\alpha t - 2\alpha tan^{-1}t}\Big) \\ \pm \frac{1}{2}\sqrt{\begin{aligned} &4A^2 - \frac{4A(9+4w)}{-9+2w} + \frac{4A\sqrt{-243+144w+16w^2}}{-9+2w} \\ &\quad + \frac{Z^2}{(t+\alpha t-2\alpha tan^{-1}t)^2} + T_3 + 4X_1 \end{aligned}} \tag{45}$$

$$\lambda_3 = \frac{A((1+\alpha)t + 2\alpha tan^{-1}t)\Lambda}{6}, \tag{46}$$

where $T_1 = -9 - 4w + \sqrt{-243+144w+16w^2}$,
$T_2 = 4A^2\epsilon_2^2 + \frac{2\epsilon_1 Z(\epsilon_1(-9-4w+\sqrt{-243+144w+16w^2})+2A(-9+2w)\epsilon_2)}{(-9+2w)(t+\alpha t-2\alpha tan^{-1}t)}$, and
$T_3 = \frac{2(-9-4w+2A(-9+2w)+\sqrt{-243+144w+16w^2})Z}{(-9+2w)(t+\alpha t-2\alpha tan^{-1}t)}$.

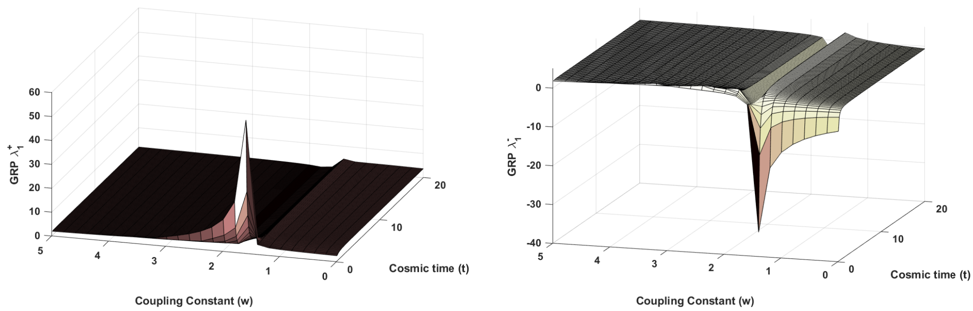

Fig. 10: λ_1^+ and λ_1^- visualizations with respect to cosmic time (t) and coupling constant w.

In Case-3, with $\beta = \frac{-4w-9}{9-2w} + \frac{1}{9-2w}\sqrt{(4w+9)^2-(9-2w)36}$, Figs. 10, 11, and 12 show the behaviour of all five GRPs over cosmic time. From the graphical analysis, the parameters λ_1^+ and λ_2^+ remain positive throughout the considered cosmic interval, indicating continuously growing perturbation modes and hence persistent instability in the corresponding perturbation sectors. On the other hand, λ_1^- and λ_2^- exhibit a transition from positive to negative values as cosmic time increases. This behaviour shows that these modes are unstable during the early cosmic phase but gradually evolve toward stability at later times due to the exponential decay of perturbations.

The GRP λ_3 initially attains negative values, corresponding to an early-time stable phase, but later becomes positive, indicating the emergence of instability during the late-time evolution of the model. This behaviour reflects the dynamical influence of the adopted FQDP on the perturbation structure of the BD framework.

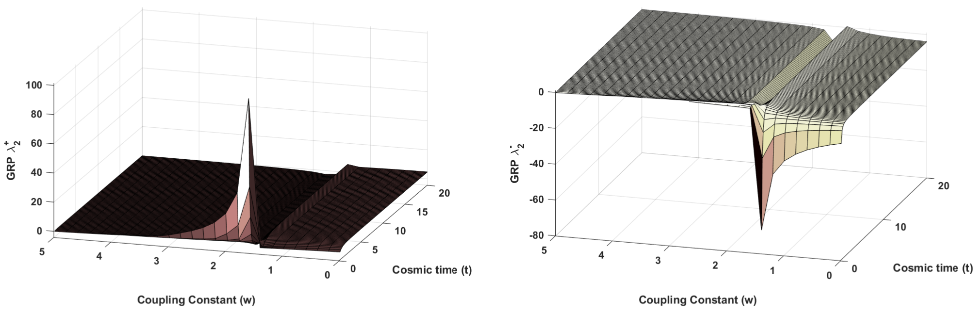

Fig. 11: λ_2^+ & λ_2^-'s visualization w.r.t cosmic time (t) and coupling constant w.

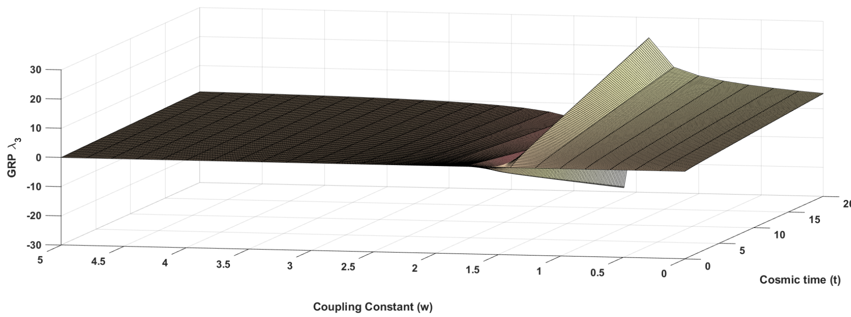

Fig. 12: λ_3's visualization w.r.t cosmic time (t) and coupling constant w.

Therefore, although some perturbation modes eventually decay during specific cosmic intervals, the persistence of positive GRPs implies that the condition $\text{Re}(\lambda_i) < 0$ is not satisfied simultaneously for all modes. Hence, Case-3 cannot be regarded as completely stable and instead represents a dynamically unstable cosmological configuration with transient stable behaviour in certain perturbation sectors.

Case 4: For $\boldsymbol{\beta = \frac{-4w-9}{9-2w} - \frac{1}{9-2w}\sqrt{(4w+9)^2 - (9-2w)36}}$

Using $\beta = \frac{-4w-9}{9-2w} - \frac{1}{9-2w}\sqrt{(4w+9)^2 - (9-2w)36}$ and substituting the values of a and $\frac{\dot{a}}{a}$ into the Eqs. (18)-(20), and solving for the GRPs $\lambda_1^{\pm}, \lambda_2^{\pm}$, and λ_3, we obtain the following expressions

$$\lambda_1^{\pm} = \frac{1}{4}\left(1+\sqrt{9+6w} - \frac{Z}{t+\alpha t - 2\alpha tan^{-1}t} - \frac{2A\epsilon_2}{\epsilon_1}\right) \pm \frac{1}{4\epsilon_1}\sqrt{\epsilon_1^2\left(\frac{(9+4w+\sqrt{-243+144w+16w^2})^2}{(9-2w)^2}+4X_1\right) + \frac{\epsilon_1^2 Z^2}{(t+\alpha t-2\alpha tan^{-1}t)^2} - \frac{4\epsilon_1 A(T_4)\epsilon_2}{-9+2w}+T_5} \tag{47}$$

$$\lambda_2^{\pm} = \frac{1}{2}\left(-2A+\frac{9+4w}{-9+2w}+\frac{\sqrt{-243+144w+16w^2}}{9-2w}-\frac{Z}{t+\alpha t-2\alpha tan^{-1}t}\right) \pm \frac{1}{2}\sqrt{4A^2-\frac{4A(9+4w)}{-9+2w}+\frac{4A\sqrt{-243+144w+16w^2}}{9-2w} + \frac{Z^2}{(t+\alpha t-2\alpha tan^{-1}t)^2}-T_6+4X_1} \tag{48}$$

$$\lambda_3 = \frac{A((1+\alpha)t+2\alpha tan^{-1}t)\Lambda}{6} \tag{49}$$

where $T_4 = 9+4w+\sqrt{-243+144w+16w^2}$,
$T_5 = 4A^2\epsilon_2^2 - \frac{2\epsilon_1 Z(\epsilon_1(9+4w+\sqrt{-243+144w+16w^2})+2A(-9+2w)\epsilon_2)}{(-9+2w)(t+\alpha t-2\alpha tan^{-1}t)}$, and
$T_6 = \frac{2(9+4w+A(18-4w)+\sqrt{-243+144w+16w^2})Z}{(-9+2w)(t+\alpha t-2\alpha tan^{-1}t)}$.

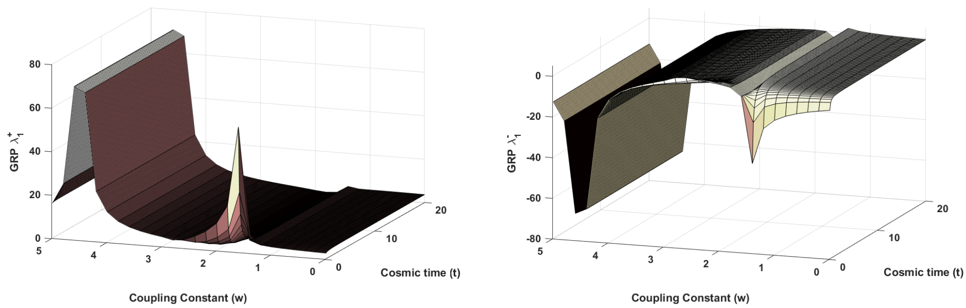

Fig. 13: λ_1^+ and λ_1^- visualizations with respect to cosmic time (t) and coupling constant w.

In Case-4, for $\beta = \frac{-4w-9}{9-2w} - \frac{1}{9-2w}\sqrt{(4w+9)^2-36(9-2w)}$, Figs. 13, 14, and 15 show how the five GRPs change with cosmic time. The values λ_1^+ and λ_2^+ stay positive across the entire time span, meaning that the related modes remain unstable and their disturbances grow continuously. These results suggest difficulty for the system to reach full stability in those directions. On the other hand, λ_1^- and λ_2^- stay negative over time, ensuring stability for their associated directions by decreasing disturbances.

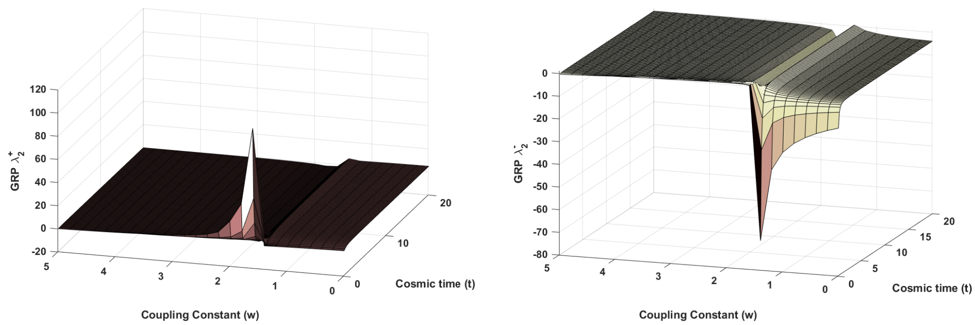

Fig. 14: λ_2^+ & λ_2^-'s visualization w.r.t cosmic time (t) and coupling constant w.

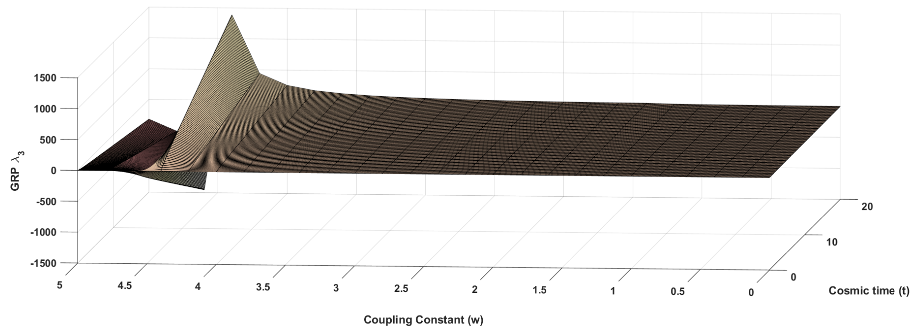

Fig. 15: λ_3's visualization w.r.t cosmic time (t) and coupling constant w.

The third growth rate, λ_3, behaves differently: it is negative early on, indicating early-time stability, but becomes positive as time increases, introducing later instability in that direction. This shows that the stability in the system can change as the universe evolves. The variation in GRP signs highlights that while certain parts of the system stay stable, others show instability that either stays or changes with time.

Overall, the stability behaviour of the system is governed by a mixed evolution of the GRPs over cosmic time. The parameters λ_1^- and λ_2^- remain negative throughout, ensuring stable perturbation decay along those modes, whereas λ_1^+ and λ_2^+ remain positive, indicating persistent instability due to continuously growing perturbations. The transition of λ_3 from negative values at early cosmic times to positive values at later stages further demonstrates that the stability structure evolves dynamically as the universe expands. Since the condition $\text{Re}(\lambda_i) < 0$ is not satisfied simultaneously for all perturbation modes, Case-4 does not correspond to a completely stable cosmological configuration, although transient stability is observed in specific perturbation sectors during the early phase of evolution.

Hence, the choice $\beta = 3 + 3\sqrt{1 + \frac{2w}{3}}$, leads to physically acceptable and dynamically stable behaviour of the cosmological model. Since all GRPs eventually satisfy the condition $\mathrm{Re}(\lambda_i) < 0$ at late cosmic times, the corresponding perturbations decay exponentially and the cosmological system asymptotically approaches equilibrium. Therefore, among all the considered cases, Case-1 provides the most physically viable and dynamically stable cosmological configuration within the present nonlinear perturbative framework.

6 Conclusions

This study presents a comprehensive framework for analyzing the dynamical stability of cosmological models within the context of the FQDP by examining the evolution of GRPs under different parametric configurations. In addition, the proposed model was statistically validated using recent observational Hubble parameter $H(z)$ data. The numerical reconstruction of $H(z)$, obtained through coupled differential equations and constrained via χ^2 minimization and MCMC techniques, yields best-fit parameter values consistent with current observational bounds. For the specific FQDP parametrization adopted in this work, the observational analysis yields the best-fit values $\alpha = 0.09$ and $H_0 = 63.608\ \mathrm{km\,s^{-1}Mpc^{-1}}$. Using these best-fit parameters, the reduced chi-square parameter together with the AIC and BIC diagnostics indicates that the model provides a statistically acceptable fit to the observational data and exhibits observational performance comparable to that of the standard ΛCDM scenario. Furthermore, the MCMC analysis yields $\alpha = -0.0202 \pm 0.1356$ and $H_0 = 62.083 \pm 2.881\ \mathrm{km\,s^{-1}Mpc^{-1}}$, with the posterior distributions lying well within the 1σ–3σ confidence regions, thereby supporting the robustness of the observational reconstruction. The best-fit value $\alpha = 0.09$ was subsequently adopted for the GRP-based stability analysis.

The investigation further demonstrates that the stability of the system is strongly governed by the interplay between the model parameters, initial conditions, and the temporal evolution of the GRPs. The main findings of the present study are summarized as follows:

- Case 1 exhibits complete dynamical stability, as all GRPs asymptotically attain negative values with cosmic time, ensuring the exponential decay of perturbations and the gradual restoration of equilibrium. This behaviour identifies Case 1 as the most physically viable and dynamically stable configuration for cosmological evolution within the present perturbative framework.
- Case 2 corresponds to an unstable cosmological configuration in which certain GRPs remain negative throughout the cosmic evolution, while others, particularly λ_3, initially exhibit instability before approaching stability at later times. Although some perturbation modes stabilize dynamically, persistent instabilities remain in other sectors of the system.
- Case 3 and Case 4 exhibit strongly time-dependent and mode-sensitive behaviour. In these cases, some GRPs remain positive throughout the cosmic evolution, indicating persistent instability in the corresponding perturbation modes, whereas others undergo transitions between stable and

unstable phases. This mixed behaviour demonstrates the strong sensitivity of the cosmological dynamics to the adopted parameter choices and perturbative structure.

Overall, the combined analytical and observational investigation establishes that cosmological stability in FQDP-based models is highly sensitive to the choice of model parameters and the behaviour of the GRPs. Among all the considered cases, Case 1 provides a fully stable and observationally consistent cosmological configuration within the Brans–Dicke framework under nonlinear perturbations. The remaining cases reveal a complex interplay between stable and unstable perturbation modes, emphasizing the intricate and time-dependent nature of cosmic dynamics. Therefore, the present study provides deeper insight into the conditional aspects of cosmological stability and further strengthens the physical viability of the proposed framework when confronted with current observational data.

References

Akarsu, Ö., Dereli, T., 2012, *Int. J. Theor. Phys.* 51, 612–621
Anderson, L., et al., 2012, *Mon. Not. R. Astron. Soc.* 427, 3435–3467
Bennett, C. L., et al., 2003, *Astrophys. J.* 583, 1
Bernardeau, F., et al., 2002, *Phys. Rep.* 367, 1–248
Berman, M. S., Mello, Gomide F., 1988, *Gen. Rel. Grav.* 20, 191–198
Brans, C., Dicke, R. H., 1961, *Phys. Rev.* 124, 925
Collaboration P., et al., 2014, *A&A* 571, 16
Debono, I., Smoot, G. F., 2016, *Univ.* 2, 23
Dhawan, S., Jha, S. W., Leibundgut, B., 2018, *Astron. Astrophys.* 609, A72
Galbany, L., de Jaeger, T., Riess, A. G., 2023, *Astron. Astrophys.* 679, A79
Harko, T., et al., 2011, *Phys. Rev. D* 84, 024020
Hayashi, K., Shirafuji, T., 1979, *Phys. Rev. D* 19, 3524
Hinshaw, G., et al., 2013, *Astrophys. J. Suppl. Ser.* 208, 19
Huang, C. D., et al., 2020, *Astrophys. J.* 889, 5
Jain, N., Mishra, R. K., 2025a, *Astrophys. Space Sci.* 370, 89
Jain, N., Mishra, R. K., 2025b, *Mod. Phys. Lett. A* 40, 2550147
Jain, N., Mishra, R. K., 2025c, *Bulg. J. Phys.* 52, 383
Jain, N., Mishra, R. K., 2026a, *Int. J. Geom. Methods Mod. Phys.* 23, 2550245
Jain, N., Mishra, R. K., 2026b, *Int. J. Mod. Phys. D* 35, 2650008
Jain, N., Dua, H., Mishra, R., 2023, *J. Phys. Conf. Ser.* 2663, 012056
Johri, V. B., Desikan, K., 1994, *Gen. Rel. Grav.* 26, 1217–1232
Kirshner, R. P., 2004, *Proc. Natl. Acad. Sci.* 101, 8–13
Lazkoz, R., et al., 2019, *Phys. Rev. D* 100, 104027
Lifshitz, E. M., 1946, *J. Phys.* 10, 116–129
Lu, J., et al., 2019, *Eur. Phys. J. Plus* 134, 318
Mandal, S., Sahoo, P. K., Santos, J. R. L., 2019, *Phys. Rev. D* 102, 024057
Mishra, R. K., Jain, N., 2024a, *Gen. Rel. Grav.* 56, 26
Mishra, R. K., Jain, N., 2024b, *Rom. J. Phys.* 69, 113
Mishra, R. K., Jain, N., 2025, *Int. J. Geom. Methods Mod. Phys.* 22, 2450310
Mishra, R. K., Sharma, R., 2025, *Mod. Phys. Lett. A* 40, 2550086
Moresco, M., et al., 2022, *Living Rev. Relativ.* 25, 6
Nariai, H., 1969, *Prog. Theor. Phys.* 42, 544–554
Perlmutter, S., et al., 1999, *Astrophys. J.* 517, 565
Rama, S. K., 1996, *Phys. Lett. B* 373, 282–288
Rama, S. K., Ghosh, S., 1996, *Phys. Lett. B* 383, 31–38
Reddy, D., Vijaya, Lakshmi G., 2015, *Astrophys. Space Sci.* 357, 1–5
Riess, A. G., et al., 1998, *Astron. J.* 116, 1009
Saez, D., Ballester, V., 1986, *Phys. Lett. A* 113, 467–470
Sharma, R., Mishra, R. K., 2026a, *Mod. Phys. Lett. A* 41, 2650017
Sharma, R., Mishra, R. K., 2026b, *Astrophys. Space Sci.* 371, 26

Sharma, R., Mishra, R. K., 2026c, *Phys. Lett. A* 586, 131681
Sharma, R., Mishra, R. K., 2026d, *Int. J. Mod. Phys. A* 41, 2650046
Sotiriou, T. P., Faraoni, V., 2010, *Rev. Mod. Phys.* 82, 451–497
Springel, V., Frenk, C. S., White, S. D., 2006, *Nature* 440, 1137–1144
Suzuki, N., et al., 2012, *Astrophys. J.* 746, 85
Thirring, W. E., 1961, *Ann. Phys.* 16, 96–117